Materials Research Proceedings 41 (2024) 1215-1223 https://doi.org/10.21741/9781644903131-135

A temperature-dependent crystal plasticity model for predicting cyclic loading behaviors of a magnesium alloy

BONG Hyuk Jong[1,a*]

[1]Materials Deformation Department, Korea Institute of Materials Science, Changwon 51508, Republic of Korea

[a]hjbong@kims.re.kr

Keywords: Crystal Plasticity, Magnesium Alloy, Cyclic Loading, Twin-Detwin

Abstract. In this work, a crystal plasticity finite element (CPFE) model to predict cyclic loading behaviors at elevated temperatures of a wrought magnesium alloy, i.e., AZ31B sheet, is proposed. The temperature-dependent mechanical behavior is systematically modeled by modifying the strain-hardening model. The twinning-detwinning, a key deformation mechanism that occurs during the cyclic loadings in the magnesium sheet, is also modeled based on the well-known predominant twinning reorientation (PTR) scheme. Furthermore, to better predict the detwinning behavior, a concept of residual twin is also introduced and employed in the PTR scheme. The modified strain-hardening and enhanced-PTR model considering the twinning-detwinning are implemented in the CPFE framework. Using the developed model, mechanical responses of the AZ31B sheet under cyclic loading conditions at various testing temperatures up to 200°C are predicted and compared with the experimental data, and the prediction results are promising.

Introduction

Magnesium and its alloys are the lightest structural metallic material and attract more attention as a lightweight material. However, the wide application of magnesium alloys is hindered by their poor formability at room temperature (RT) due to the limited number of independent deformation mechanisms [1]. However, non-basal slip systems become more active at higher temperatures since their critical resolved shear stresses (CRSSs), known to be significant temperature dependent [2–4], decrease, and they can accommodate the plastic deformation with other slip or twin systems of magnesium alloys with its hexagonal close-packed (HCP) crystal structure.

To overcome the limited formability and asymmetric mechanical responses of magnesium alloy sheets at room temperature, temperature-assisted forming of such alloys is widely employed. Therefore, the material modeling for the magnesium alloy sheets considering complicated slip and twin mechanisms under elevated temperature conditions as well as strain-path changes is vital.

Crystal plasticity is useful for understanding underlying deformation mechanisms and predicting micro- and macro-properties as a consequence of such deformation mechanisms. To date, the crystal plasticity models consider the heterogeneous CRSSs of available slip and twin systems for the HCP-structured magnesium alloys [5–9]. Among them, several attempts have been made to model the temperature-dependent mechanical responses [7,10]. In addition, the crystal plasticity models to predict abnormal mechanical responses under the cyclic loading scenarios considering the twinning-detwinning phenomenon have been proposed [8,9]. However, a material model based on a crystal plasticity framework for cyclic loading scenarios at elevated temperatures for magnesium alloys has not been proposed yet.

The main focus of the current work is to develop a CPFE model that can reproduce the mechanical responses of HCP-structured magnesium (and its alloys) under various temperatures and cyclic loading scenarios at the same time. In the newly developed model, there are two main advancements compared to conventional CPFE model: (a) the temperature dependency of non-basal slip systems is systematically modeled by modifying the strain-hardening model, i.e.,

extended Voce hardening, as a function of temperature, and (b) the well-known predominant twinning reorientation (PTR) scheme is enhanced by incorporating the twinning-detwinning mechanism and introducing the concept of residual twin as a criterion for detwinning termination.

Materials

A commercially available AZ31B magnesium alloy sheet with a thickness of 1.4 mm is investigated in the current study. The chemical composition of the corresponding magnesium alloy is listed in Table 1.

Table 1. Chemical composition of AZ31B sheet (unit in wt%)

Al	Zn	Mn	Si	Fe	Cu	Mg
2.5-3.5	0.6-1.4	0.2-1.0	<0.1	<0.005	<0.05	Balance

To obtain the initial crystallographic texture of the AZ31B, an X-ray diffraction test was conducted. Using the measured pole figures shown in Fig. 1, the orientation distribution function (ODF) was estimated, and 1,000 discrete Euler angles were extracted from the estimated ODF. They were then used as input for the CPFE simulation afterward.

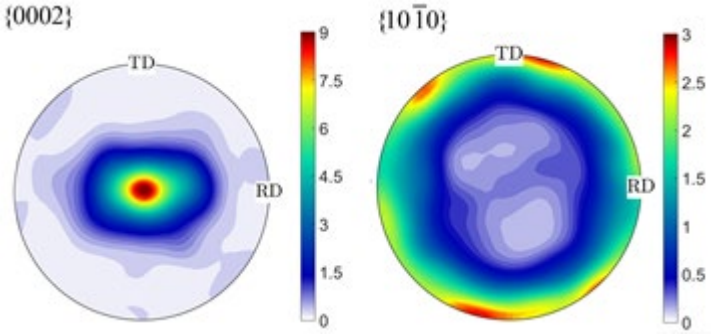

Fig. 1. $\{\mathbf{0002}\}$ *and* $\{\mathbf{10\bar{1}0}\}$ *pole figures of as-received AZ31B sheet measured by X-ray diffraction*

Experimental

Uniaxial tension tests of the AZ31B sheet were conducted using an ASTM E8 specimen with a gauge length of 25 mm. The samples were heated up using a heating chamber. The strain fields were measured using the ARAMIS digital image correlation (DIC) system, and recorded images were analyzed to obtain stress-strain data along with the load data from the universal testing machine and r-value defined as $\mathrm{r} = -\varepsilon_W/(\varepsilon_W + \varepsilon_L)$. The r-value is calculated from the recorded DIC image during the test.

The mechanical responses under the cyclic loading conditions were obtained by conducting in-plane cyclic tests. The testing apparatus and dimensions of the testing sample are shown in Fig. 2. The clamping dies were heated up using cartridge heaters. The temperature of the sample was measured using attached thermocouples and tests were initiated once the target temperature of the sample was reached. Out-of-plane buckling was prevented by applying side force to the anti-buckling plates of 2 kN for tests at RT and 100 °C and 1 kN for the tests at 150 and 200 °C. The biaxial stress induced by the side force and frictional force between the anti-buckling plates and the sample was corrected according to the procedure reported elsewhere [11]. Using the sample testing apparatus, the in-plane uniaxial tension tests were also conducted at the same temperature conditions.

The uniaxial tension, uniaxial compression, and cyclic tests were conducted along the rolling direction at a strain rate of ~0.001/s and RT, 100, 150, and 200 °C.

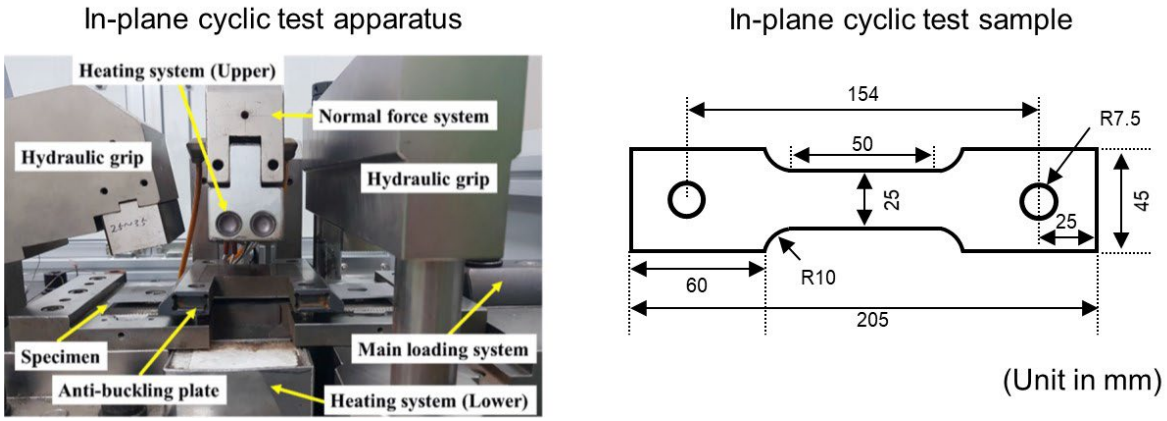

Fig. 2. In-plane cyclic testing apparatus and dimension of testing sample

Crystal plasticity modeling

A CPFE model to model temperature dependency under cyclic loading conditions based on a rate-dependent crystal plasticity framework [12,13] was developed. The basic formulations of the crystal plasticity for the HCP-structured metallic materials can be found elsewhere [5], and only a summary of the CPFE model is presented in this section along with the core formulation for the temperature-dependency and twinning-detwinning model [14].

The temperature dependency of the non-basal slip systems is addressed by modifying the Voce hardening model as

$$\tau_{crss}^{\alpha}(T,\Gamma) = \tau_0^{\alpha}(T) + (\tau_1^{\alpha}(T) + \theta_1^{\alpha}(T)\cdot\Gamma)\left\{1 - exp\left(-\frac{\theta_0^{\alpha}(T)\cdot\Gamma}{\tau_1^{\alpha}(T)}\right)\right\} \quad (1)$$

where Γ is the total accumulated shear strain over all available slip and twin systems, and $\tau_0^{\alpha}(T)$, $\tau_1^{\alpha}(T)$, $\theta_0^{\alpha}(T)$, and $\theta_1^{\alpha}(T)$ are temperature-dependent hardening parameters of α-th non-basal slip systems and they are modeled as follows according to Singh et al. [15]:

$$\begin{pmatrix}\tau_0^{\alpha}(T)\\ \tau_1^{\alpha}(T)\\ \theta_0^{\alpha}(T)\\ \theta_1^{\alpha}(T)\end{pmatrix} = \mathrm{k}(T)\begin{pmatrix}\tau_0^{\alpha}(T_R)\\ \tau_1^{\alpha}(T_R)\\ \theta_0^{\alpha}(T_R)\\ \theta_1^{\alpha}(T_R)\end{pmatrix} \quad (2)$$

where T_R is the reference temperature, and $\mathrm{k}(T)$ is the temperature-dependent scaling factor.

Twinning-detwinning based on the PTR scheme is proposed, and the details are elsewhere [14]. Here, only a flowchart describing the activation of twinning and detwinning is presented in Fig. 3. According to the PTR model, when the volume fraction of twins in a particular grain exceeds the threshold value f_c, that grain will be re-orientated. f_c evolves as

$$f_c = min\left(1.0, A + B\frac{F_E}{F_A}\right) \quad (3)$$

where $F_E\left(=\sum_{m=1}^{NG^{twin}} w^m\right)$ is the effective twin volume fraction and $F_A\left(=\sum_{n=1}^{NG}\left(w^n\sum_{\beta=1}^{N^{TW}} f^{\beta}\right)\right)$. Here, NG^{twin}, NG, and w, N^{twin} are the total number of fully twinned grains, total number of grains, volume fraction of the corresponding grains overall grains, and numbers of twin variants, respectively.

The basic assumption of the proposed twinning-detwinning model is that only one of two, i.e., twin and detwin, will be active during each loading step. It is worthwhile to note that slip systems

are active at all time steps. During the first loading, the twin should be active. Then, at the onset of the second loading, the grains are categorized into the following three different twinning-detwinning scenarios according to the twin volume fraction. In Case I, the volume fraction exceeds the threshold at the first loading and the grain is completely re-oriented. In such a case, it can be assumed that detwinning is activated at the second loading. In Case II, the grain is not completely re-oriented at the first loading, but some amount of twin is created more than f_r, the residual twin fraction. The residual twin represents persisting twins, even after full reverse loading. If the fraction of twin generated at first loading is greater than f_r, detwin will be activated during the second loading, otherwise this Case III is assumed. In this case, the grain does not have the right orientation for the twin to take place, and the twin is activated during the second loading. During the next loading sequence, twin occurs again in the grain that is detwinned at the second loading. However, in Case III in the second loading, the three cases can be assumed again as shown in Fig. 3.

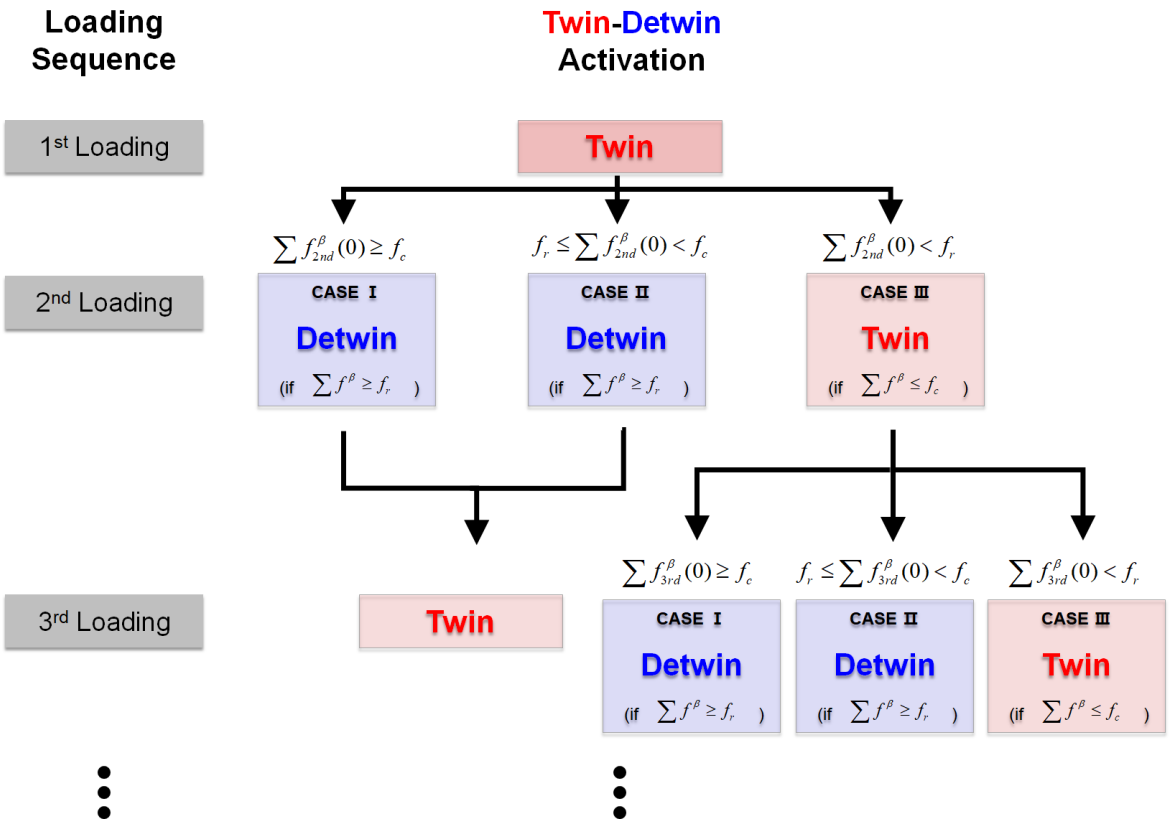

Fig. 3. Flowchart of proposed twinning-detwinning model [14].

Results

The material parameters are identified by simultaneously fitting using a representative volume element (RVE) incorporated with the developed CPFE model to stress-strain curves obtained from the uniaxial tension and compression tests, and (accumulated) r-value obtained from the uniaxial tension tests at all investigated testing temperatures. The RVE model consists of 1,000 finite elements (FEs) represented by 8-node brick element with reduced integration. Each FE represents a single crystal, and thus, the RVE represents a polycrystal with 1,000 grains. Periodic boundary condition is imposed as described in previous studies by the author [16,17]. The following four slip/twin systems are assumed to be active: $\{\mathbf{0001}\}\langle\mathbf{11\bar{2}0}\rangle$ basal slip, $\{\mathbf{10\bar{1}1}\}\langle\mathbf{11\bar{2}0}\rangle$ prismatic slip, $\{\mathbf{11\bar{2}2}\}\langle\mathbf{11\bar{2}3}\rangle$ pyramidal <a+c> slip, and $\{\mathbf{10\bar{1}2}\}\langle\mathbf{\bar{1}011}\rangle$ tensile twin.

The fitting results are shown in Fig. 4. The identified constitutive parameters for the extended Voce hardening model are listed in Table 2. The PTR model parameters in Eq. (3) are identified as A=0.7 and B=1 for all the testing temperatures. It is worthwhile to note that the Voce hardening parameters for the tensile detwin are identified by fitting to the cyclic loading data obtained from the in-plane cyclic tests, which will appear later on.

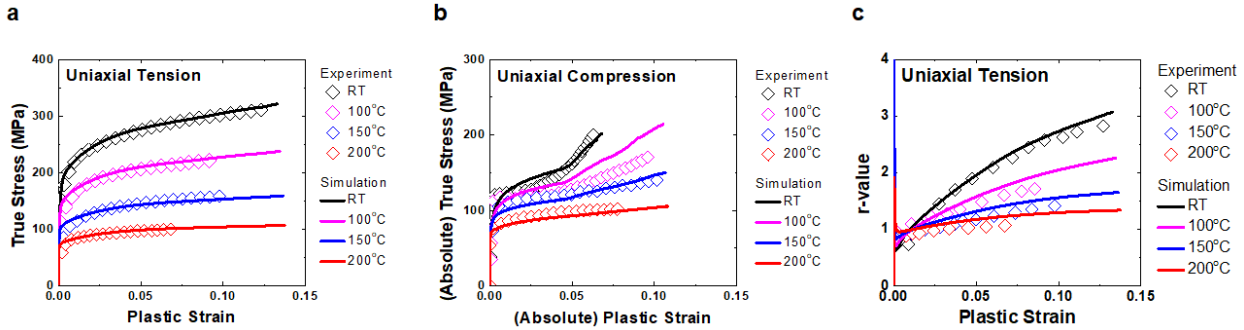

Fig. 4. Measured and simulated stress-strain curves under (a) uniaxial tension and (b) uniaxial compression, and (c) r-values under uniaxial tension

Table 2 Identified constitutive parameters for the extended Voce hardening model

Temperature	Slip/Twin Systems	τ_0	τ_1	θ_0	θ_1	q_{ij}
25	Basal	25	1	90	0	2.5
	Prismatic	105	21	390	10	2.5
	Pyramidal <a+c>	108	29	440	15	4
	Tensile twin	28	5	10	5	2.5
	Tensile detwin	21	5	10	5	2.5
100	Basal	25	1	90	0	2.5
	Prismatic	74	16	280	7.5	2.5
	Pyramidal <a+c>	76	20.5	320	11	4
	Tensile twin	28	5	10	5	2.5
	Tensile detwin	21	5	10	5	2.5
150	Basal	25	1	90	0	2.5
	Prismatic	50	12	185	6	2.5
	Pyramidal <a+c>	51	15	210	8.5	4
	Tensile twin	28	5	10	5	2.5
	Tensile detwin	21	5	10	5	2.5
200	Basal	25	1	90	0	2.5
	Prismatic	33	7	130	3	2.5
	Pyramidal <a+c>	34	8	140	5	4
	Tensile twin	28	5	10	5	2.5
	Tensile detwin	21	5	10	5	2.5

The scaling factor representing the temperature dependency is determined by fitting the identified Voce hardening parameters of the non-basal slip systems at different temperatures in Table 2. The hardening parameters are normalized to those at a reference temperature, i.e., RT. The normalized hardening parameters are fitted using a phenomenological equation, $k(T) = 1/\left(1 + \left((T - T_R)/h_1\right)^{h_2}\right)$ as h_1=124 and h_2= 2.05. The normalized hardening parameters and the fitted curve are shown in Fig. 5.

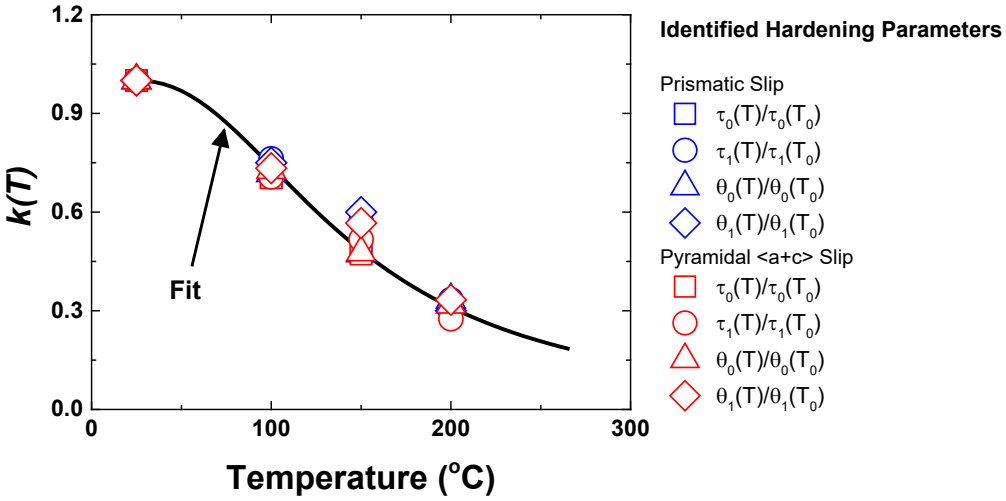

Fig. 5. Normalized Voce hardening parameters for non-basal slip systems at different temperatures and best-fit

The stress-strain curves under cyclic loadings, namely, compression-tension-compression (CTC) and tension-compression-tension (TCT), at RT, 100, 150, and 200°C are predicted using identified constitutive parameters and compared with the experimental data. The results are shown in Fig. 6.

During the first loading step in TCT, the tensile twin is hardly active. Therefore, the stress-strain curve is concave down shaped. During the second loading step, a stress plateau is observed at the beginning since the tensile twin is active. However, as the twin activation is terminated, non-basal slip systems are supposed to be active. Therefore, a concave down-shaped stress-strain curve is observed. During the third loading step, detwinning should be active in twinned areas during the second loading step, and a concave-up shaped stress-strain curve is observed with the stress plateau at the beginning. A similar phenomenon in terms of the stress-strain curve in consequence of twin and detwin activation in CTC. The CPFE well reproduce such abnormal stress-strain curves. The predictions at higher temperatures are also presented in Fig. 6, and the predictions are in good agreement with the measured data.

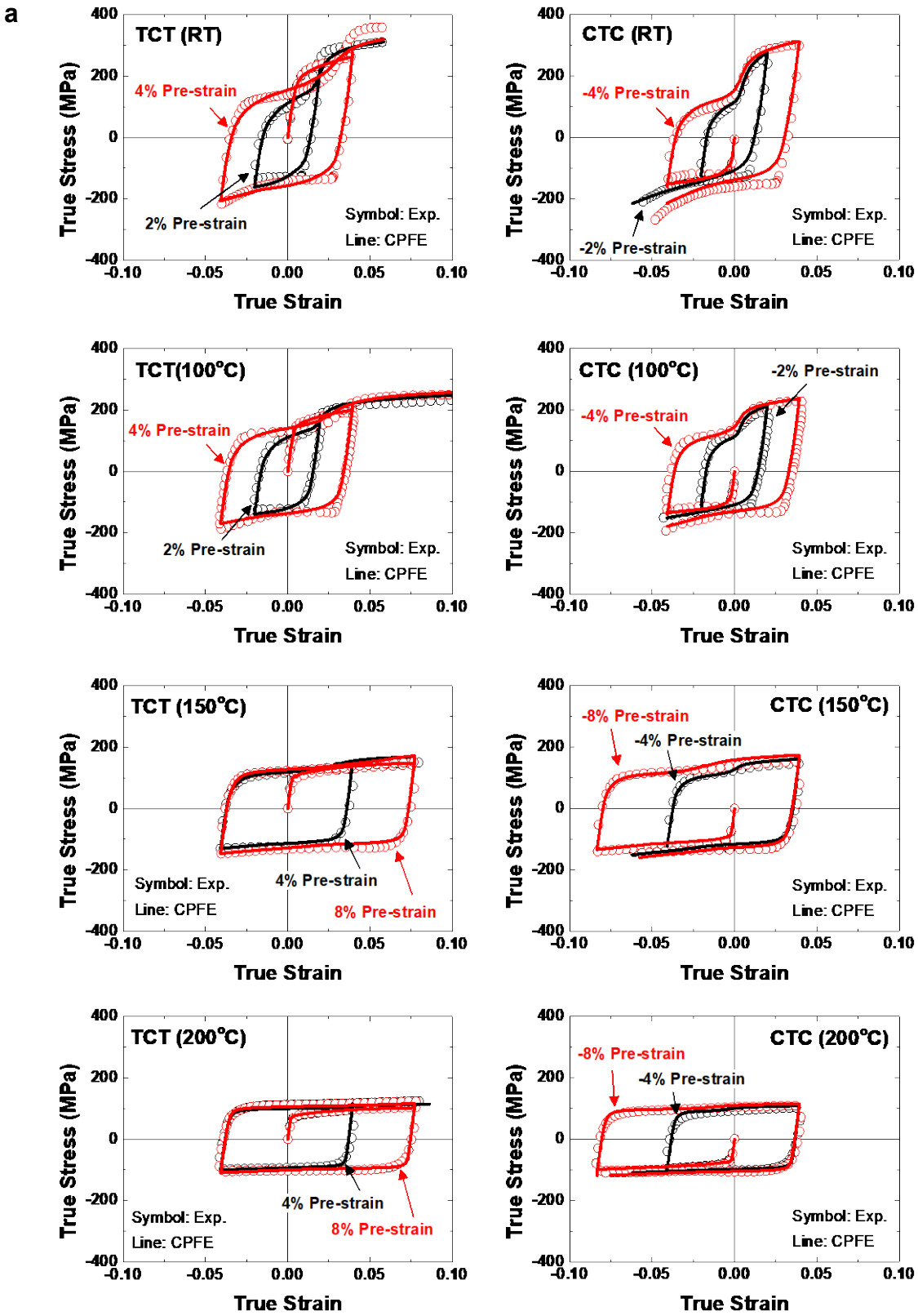

Fig. 6. Measured and predicted stress-strain curves under cyclic loading conditions at (a) RT, (b) 100°C, (c) 150°C, and (d) 200°C

Summary
In the current work, a CPFE model to predict the mechanical behaviors of a magnesium alloy sheet under different temperature conditions and cyclic loading scenarios is developed. For such, the temperature dependency of the non-basal slip systems is modeled systematically by modifying the Voce hardening model, and the predominant twinning reorientation (PTR) scheme is further enhanced by incorporating the twinning-detwinning mechanism. The newly developed crystal plasticity model is applied in predicting mechanical responses under in-plane tensile loadings, compressive loadings, and cyclic loadings at different temperatures up to 200 °C. Finally, the predictions are compared with measured ones. The proposed model reproduces stress-strain responses under not only monotonic loadings but also cyclic loadings at various testing temperatures from room temperature to 200°C.

Acknowledgments
This work was supported by the Fundamental Research Program of the Korea Institute of Materials Science (KIMS, PNK9800) and the National Research Council of Science and Technology (NST) grant by the Korea government (MSIT) (CRC23011-210).

References

[1] S.A. Habib, A.S. Khan, T. Gnäupel-Herold, J.T. Lloyd, S.E. Schoenfeld, Anisotropy, tension-compression asymmetry and texture evolution of a rare-earth-containing magnesium alloy sheet, ZEK100, at different strain rates and temperatures: Experiments and modeling, Int. J. Plast. 95 (2017) 163–190. https://doi.org/https://doi.org/10.1016/j.ijplas.2017.04.006

[2] H. Yoshinaga, R. Horiuchi, On the Nonbasal Slip in Magnesium Crystals, Trans. Japan Inst. Met. 5 (1964) 14–21. https://doi.org/10.2320/matertrans1960.5.14

[3] T. Obara, H. Yoshinga, S. Morozumi, {11$\bar{2}$2}〈1123〉 Slip system in magnesium, Acta Metall. 21 (1973) 845–853. https://doi.org/https://doi.org/10.1016/0001-6160(73)90141-7

[4] S.R. Agnew, Ö. Duygulu, Plastic anisotropy and the role of non-basal slip in magnesium alloy AZ31B, Int. J. Plast. 21 (2005) 1161–1193. https://doi.org/https://doi.org/10.1016/j.ijplas.2004.05.018

[5] H.J. Bong, X. Hu, X. Sun, Y. Ren, Mechanism-based constitutive modeling of ZEK100 magnesium alloy with crystal plasticity and in-situ HEXRD experiment, Int. J. Plast. 113 (2019) 35–51. https://doi.org/https://doi.org/10.1016/j.ijplas.2018.09.005

[6] H.J. Bong, J. Lee, X. Hu, X. Sun, M.-G. Lee, Predicting forming limit diagrams for magnesium alloys using crystal plasticity finite elements, Int. J. Plast. 126 (2020) 102630. https://doi.org/https://doi.org/10.1016/j.ijplas.2019.11.009

[7] A. Jain, S.R. Agnew, Modeling the temperature dependent effect of twinning on the behavior of magnesium alloy AZ31B sheet, Mater. Sci. Eng. A. 462 (2007) 29–36. https://doi.org/https://doi.org/10.1016/j.msea.2006.03.160

[8] H. Wang, P.D. Wu, J. Wang, Modeling inelastic behavior of magnesium alloys during cyclic loading–unloading, Int. J. Plast. 47 (2013) 49–64. https://doi.org/10.1016/j.ijplas.2013.01.007

[9] H. Zhang, A. Jérusalem, E. Salvati, C. Papadaki, K.S. Fong, X. Song, A.M. Korsunsky, Multi-scale mechanisms of twinning-detwinning in magnesium alloy AZ31B simulated by crystal plasticity modeling and validated via in situ synchrotron XRD and in situ SEM-EBSD, Int. J. Plast. 119 (2019) 43–56. https://doi.org/https://doi.org/10.1016/j.ijplas.2019.02.018

[10] Q. Liu, A. Roy, V. V Silberschmidt, Temperature-dependent crystal-plasticity model for magnesium: A bottom-up approach, Mech. Mater. 113 (2017) 44–56. https://doi.org/https://doi.org/10.1016/j.mechmat.2017.07.008

[11] M.G. Lee, J.H. Kim, D. Kim, O.S. Seo, N.T. Nguyen, H.Y. Kim, Anisotropic Hardening of Sheet Metals at Elevated Temperature: Tension-Compressions Test Development and Validation, Exp. Mech. 53 (2013) 1039–1055. https://doi.org/10.1007/s11340-012-9694-1

[12] R.J. Asaro, Geometrical effects in the inhomogeneous deformation of ductile single crystals, Acta Metall. 27 (1979) 445–453. https://doi.org/10.1016/0001-6160(79)90036-1

[13] S.R. Kalidindi, C.A. Bronkhorst, L. Anand, Crystallographic texture evolution in bulk deformation processing of FCC metals, J. Mech. Phys. Solids. 40 (1992) 537–569. https://doi.org/10.1016/0022-5096(92)80003-9

[14] H.J. Bong, J. Lee, M.-G. Lee, Modeling crystal plasticity with an enhanced twinning–detwinning model to simulate cyclic behavior of AZ31B magnesium alloy at various temperatures, Int. J. Plast. 150 (2022) 103190. https://doi.org/https://doi.org/10.1016/j.ijplas.2021.103190

[15] J. Singh, S. Mahesh, S. Roy, G. Kumar, D. Srivastava, G.K. Dey, N. Saibaba, I. Samajdar, Temperature dependence of work hardening in sparsely twinning zirconium, Acta Mater. 123 (2017) 337–349. https://doi.org/https://doi.org/10.1016/j.actamat.2016.10.049

[16] H.J. Bong, J. Lee, Crystal plasticity finite element–Marciniak-Kuczynski approach with surface roughening effect in predicting formability of ultra-thin ferritic stainless steel sheets, Int. J. Mech. Sci. 191 (2021) 106066. https://doi.org/https://doi.org/10.1016/j.ijmecsci.2020.106066

[17] H.J. Bong, J. Lee, M.-G. Lee, Study on Plastic Response Under Biaxial Tension and Its Correlation with Formability for Wrought Magnesium Alloys, JOM. 72 (2020) 2568–2577. https://doi.org/10.1007/s11837-020-04084-w